Analyst

RSC Publishing

PAPER

View Article Online
View Journal | View Issue

Fabrication of Cr doped SnO_2 nanoparticles based biosensor for the selective determination of riboflavin in pharmaceuticals†

Cite this: *Analyst*, 2013, **138**, 2061

N. Lavanya,[a] S. Radhakrishnan,[a] C. Sekar,*[ab] M. Navaneethan[b] and Y. Hayakawa[b]

Received 27th November 2012
Accepted 9th January 2013

DOI: 10.1039/c3an36754a

www.rsc.org/analyst

We report the fabrication and testing of a riboflavin (RF) biosensor based on the use of Cr doped SnO_2 nanoparticles. The Cr–SnO_2 nanoparticles with chromium concentration from 0 to 5 wt% were synthesised by a microwave irradiation method. Magnetic studies revealed that only 3 wt% Cr doped nano-SnO_2 has ferromagnetic behaviour at room temperature. This Cr–SnO_2 nanoparticles modified electrode responded to RF linearly over a concentration range of 0.2×10^{-6} to 1.0×10^{-4} M with a detection limit of 107 nM. The fabricated sensor showed an excellent anti-interference ability against electroactive species and metal ions and proved to be useful for the estimation of the RF content in pharmaceutical samples with satisfactory recovery.

1 Introduction

Nanostructured metal-oxide semiconductor based nanosensors have wide applications in biological, environmental and analytical chemical sciences. Among the oxide semiconductors, tin oxide (SnO_2) is one of the most promising candidates as a host material which has been used in gas sensors, dye-sensitized solar cells, electrochromic windows, transparent conducting electrodes, transistors, catalysts, supercapacitors, and so forth.[1,2] SnO_2 is a versatile material with a wide band gap (3.6 eV at 300 K) in its stoichiometric form, but due to lattice imperfections and oxygen vacancies arising during its production, it becomes n-type and conductive.[3] SnO_2 has been of considerable interest because of its combined properties of plentiful oxygen vacancies, high optical transparency, chemical and electrochemical stability, good electrocatalytic activity, nontoxicity, good biocompatibility, and high electron communication features when doped.[4] Chemical doping with appropriate elements (Fe, Cr, Co, Mn, Ni, *etc.*) is widely used as an effective method to tune surface states, energy levels of semiconductors and transport performance of carriers, and enhance the electrical, electrochemical and magnetic properties of materials.[5] Among these, Cr is the only elemental solid which shows antiferromagnetic ordering at room temperature and below. The ionic radius of Cr(III) is close to that of Sn^{4+}, which means that Cr^{3+} can easily penetrate into the SnO_2 crystal lattice or substitute the Sn^{4+} position in the crystal.[6] Various methods have been used to synthesize the SnO_2 nanostructures; sol–gel method,[7] co-precipitation,[8] pulsed laser deposition,[9] spray pyrolysis,[10] solid state reaction method,[11] polymeric precursor's route,[12] hydrothermal method,[13] *etc.* However, it still remains a great challenge to develop a simple method for fabricating nano-SnO_2, particularly metal ion doped SnO_2 nanostructures with controlled morphology. Herein we report the synthesis of Cr doped SnO_2 nanoparticles by a simple microwave irradiation method for the first time. Microwave assisted synthesis is a clean modern technique widely used for green chemistry. It takes only a few minutes to complete the reaction and it prevents agglomeration.

Riboflavin (VB_2) is a water-soluble B-group vitamin essential to human health which helps the body convert carbohydrates, fats and proteins into energy and supports the body during the stress of daily living.[14] Riboflavin is converted to 2 coenzymes, flavin mononucleotide (FMN) and flavin adenine dinucleotide (FAD), which are necessary for normal tissue respiration. These coenzymes are involved in several reduction oxidation reactions and take part in the metabolism of other vitamins, *e.g.*, folate and vitamin B_6.[15] Riboflavin is very stable during thermal processing, storage or food preparation, but it is susceptible to degradation after exposure to light. Lack of riboflavin may lead to itching and burning eyes, sensitivity of eyes to light, sore tongue, itching and peeling skin on the nose and scrotum, and sores in the mouth. Riboflavin is found in various foods, including milk and dairy products, fish, meats, green leafy vegetables, and whole grain and enriched cereals and bread.[16] For the determination of riboflavin, several techniques have been developed, including liquid chromatography,[17] chemiluminescence,[18] spectrophotometry,[19] mass spectrometry[20] and

[a]*Department of Bioelectronics and Biosensors, Alagappa University, Karaikudi-630003, Tamilnadu, India. E-mail: Sekar2025@gmail.com; Fax: +91 4565225202; Tel: +91 94425663637*

[b]*Research Institute of Electronics, Shizuoka University, Hamamatsu-432-8011, Japan*

† Electronic supplementary information (ESI) available: XRD parameter in Table S1 and comparison of our sensor performance with literature reports in Table S2. See DOI: 10.1039/c3an36754a

fluorescence.[21] However, these methods are sometimes tedious, time consuming and involve complicated procedures and expensive instrumentation. Electrochemical methods are the most promising techniques for the detection of various analytes owing to the advantages of simplicity, high reliability, sensitivity and selectivity, low cost, fast response, and ease of use. Janik and Elving reviewed the electrochemistry of riboflavin and their work comprehensively summarises the electrochemical behaviour of the flavin nucleotides at dropping mercury electrodes (DME).[22] Various types of electrodes such as glassy carbon electrodes (GCE), plain carbon paste electrodes, solid composite electrodes, DNA and carbon nanotube mixed paste electrodes, or carbon paste electrodes modified with different compounds (*e.g.*, aza macrocycles, silica gel and sol–gel silica modified with niobium oxide, or ionic liquid) have been used for the determination of riboflavin.[23] Gu *et al.* have used voltammetric methods to determine the presence of riboflavin at electrochemically pretreated GCE.[24] Safavi *et al.* studied the electrochemical properties of riboflavin adsorbed on a carbon ionic liquid electrode (CILE) and found that the detection limit was 0.1 nM.[25] Recently Bandzuchova *et al.* investigated the electrocatalysis of riboflavin using a mercury meniscus modified electrode and polished silver amalgam electrode and obtained detection limits of 8.2×10^{-10} mol L^{-1} and 1.3×10^{-9} mol L^{-1} respectively.[26]

In this paper, we report the fabrication, characterization and analytical performances of a riboflavin sensor based on a nano-Cr–SnO_2 modified GCE by a very simple technique. Cr doped SnO_2 nanoparticles with a chromium concentration of 0 to 5 wt % were synthesized by a microwave irradiation method. The performance of the newly fabricated riboflavin sensor was studied using cyclic voltammetry (CV), electrochemical impedance spectroscopy (EIS) and differential pulse voltammetry (DPV) and the results are discussed. The fabricated sensor showed high sensitivity, good stability and satisfactory reproducibility.

2 Experimental

2.1 Materials

The reagents used were of analytical grade without further purification; $Cr(NO_3)_3 \cdot 9H_2O$ and $SnCl_2 \cdot 2H_2O$ (Fischer Scientific, Mumbai) and riboflavin (Sisco Research Laboratories, Mumbai). A 1.00×10^{-3} M stock standard solution of riboflavin was prepared by dissolving 3 mg riboflavin in 10 mL of 0.1 M phosphate buffer (pH 5.0) solution, and stored at 4 °C. 0.1 M phosphate buffer solutions (PBS) with different pH values were prepared by mixing the stock standard solutions of Na_2HPO_4 and NaH_2PO_4 and adjusting the pH with 0.1 M H_3PO_4 or NaOH. The solutions were prepared with double-distilled water.

2.2 Instrumentation

A CHI 608d & 680 electrochemical analyzer (CH Instruments, Austin, USA) connected to a glassy carbon working electrode, an Ag/AgCl (3 M KCl) reference electrode and platinum wire auxiliary electrode were used. All the solutions were deaerated with inert nitrogen gas during experiments. Cyclic voltammograms were recorded between a potential window of −0.2 V and 0.6 V at a scan rate of 50 mV s^{-1} in 0.1 M KCl containing 1.0 mM $[Fe(CN)_6]^{3-/4-}$ redox couple. The EIS measurements were carreid out by applying an ac potential of amplitude 5 mV over the dc potential of 250 mV in a frequency range of 100 kHz to 1 Hz. The DPV measurements were performed in the potential region from −0.8 to 0.2 V in PBS (pH 5.0) at a scan rate of 20 mV s^{-1} with an amplitude of 0.05 V and a step potential of 0.07 V.

The powder X-ray diffraction (XRD) patterns of the samples were recorded using a Bruker AXS D8 advanced diffractometer with Cu Kα radiation (λ = 1.5406Å) in the range of 20–80°. Surface morphology and particle size analyses were done using transmission electron microscopy (JEOL 2100 F) with an accelerating voltage of 200 keV. Magnetization measurements as a function of magnetic field (*M–H*) at room temperature up to 20 kOe were undertaken using a vibrating sample magnetometer (model: P252 Quantum Design).

2.3 Preparation and analysis of real samples

Pharmaceutical B complex and riboflavin tablets were selected for riboflavin real sample analysis. Riboflavin and B complex tablets (Shreya life sciences, Uttarakhand) were obtained from a local drugstore. Milk powder (Hatsun Agro Product Limited, Chennai) was purchased from a local supermarket. Both vitamin tablets were weighed, and then ground to a fine powder with a mortar. The powder was mixed with 100 mL of deionized water, sonicated for 30 minutes and then filtered through Whatman 42 (125 mm diameter) filter paper to yield a clear solution. The solution was diluted with PBS (pH 5.0) to the required concentration and DPV was performed using the standard additions method.

Milk powder was first weighed, and then dissolved in a small amount of boiling water; proteins present in it were precipitated out by drop wise addition of glacial acetic acid. The solution was then digested in a water bath for 20 minutes and filtered through Whatman 42 (125 mm diameter) filter paper. The pH of the diluted filtrate was adjusted with boric acid and orthophosphoric acid to pH 5.0 and the determination was performed using DPV.

2.4 Material preparation

The synthesis process of Cr doped SnO_2 nanopowders was similar to the one reported earlier.[27] Briefly, 0.1 M solution of $SnCl_2 \cdot 2H_2O$ and $Cr(NO_3)_3 \cdot 9H_2O$ with different Cr (0, 1, 3, and 5 wt%) content were mixed. Ammonium hydroxide (NH_4OH) was added drop wise (about 1 drop per 3–4 s) to the above solution until the pH reached 8. This solution was again stirred for 30 minutes to form a greenish colloidal gel. Further, the hydroxide product was washed several times with deionised water and ethanol in order to remove the Cl^- and NH^{4+} ions respectively. Then the precipitate was transferred into a microwave oven (600 W) and kept for 20 minutes. Finally, the Cr doped SnO_2 nanopowders were obtained after annealing the precipitates at 600 °C for 5 h in an ambient atmosphere.

2.5 Fabrication of the modified electrodes

Prior to modification, the bare GCE was polished with gamma alumina suspensions (1.0, 0.3 and 0.5 μM respectively). After that, the electrode was successively washed in ethanol and water for 2 minutes by ultrasonic method. The SnO_2 modified electrode was prepared by a simple drop casting method. Typically, 6 mg of the SnO_2 nanoparticles in double-distilled water (1 mL) was drop casted (10 μL) onto the GCE and air dried at room temperature for 60 minutes.

3 Results and discussion

3.1 Structural analysis

The structural properties of the undoped and Cr (1, 3, and 5 wt%) doped SnO_2 nanopowders were investigated by powder XRD method. The XRD patterns (Fig. 1) of all the samples could be indexed to (ICDD-PDF card no. 41-1445) the rutile-type phase of SnO_2 with a tetragonal unit cell which are consistent with the standard values for bulk SnO_2. No characteristic peaks of impurities, such as other forms of tin oxides, pure Sn or Cr oxides were observed within the detection sensitivity. The unit cell parameters were calculated from the known (h k l) values of the peaks (1 1 0) and (1 0 1) using the equation $1/d^2 = (h^2 + k^2)/a^2 + l^2/c^2$ and the values are presented in ESI Table S1.† The observed shrinkage of the unit cell volume is consistent with the fact that the ionic radius and valence of Cr^{3+} (63 Å) is smaller than that of Sn^{4+} (74 Å). The XRD results showed that the Cr^{3+} ions incorporate into SnO_2 lattice or replace Sn^{4+} sites without changing the rutile structure.

The average crystallite size (D) was determined using the diffraction peaks of (110) and (101) from Scherer's formula

$$D = K\lambda/\beta\cos\Theta$$

where K is the shape factor whose value is taken as 0.89, λ is the wavelength of Cu Kα radiation, and β is the corrected full width at half maximum (FWHM) of the diffraction peak and Θ is the diffracting angle. The average crystallite sizes were found to be 19, 15, 13 and 11 nm for undoped SnO_2, 1 wt%, 3 wt% and 5 wt% Cr doped SnO_2 nanoparticles respectively. These results indicate that the crystallite size of the Cr doped SnO_2 nanoparticles depends on the Cr content, and that the doping inhibits growth of crystalline grains of SnO_2.

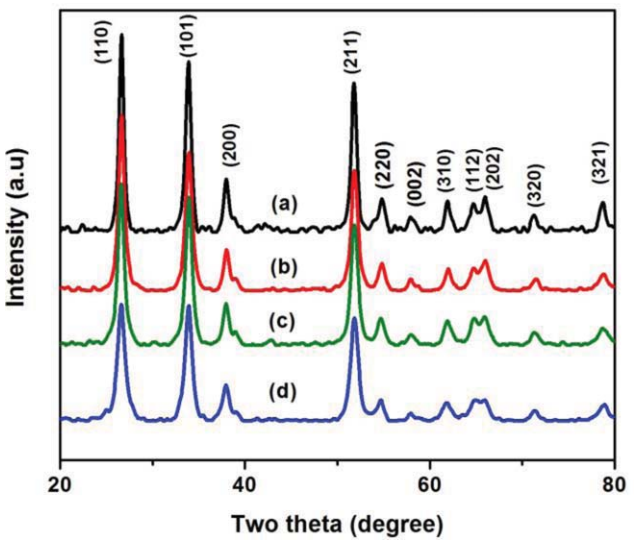

Fig. 1 XRD patterns of (a) undoped SnO_2, (b) 1 wt%, (c) 3 wt%, and (d) 5 wt% Cr doped SnO_2 nanoparticles.

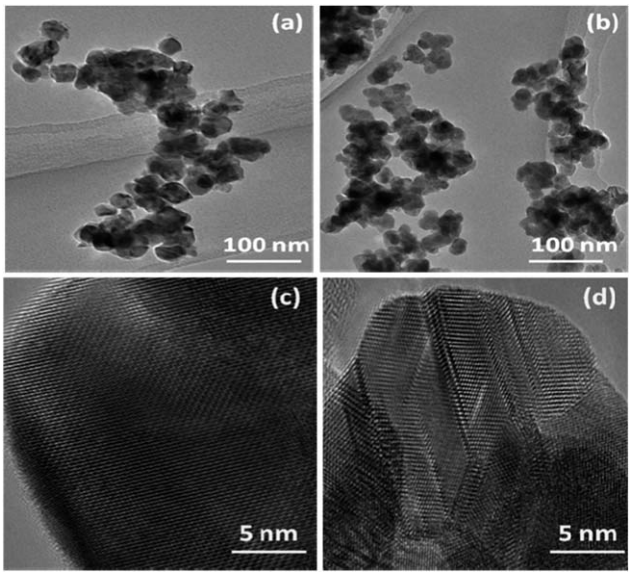

Fig. 2 TEM image of (a) undoped SnO_2, (b) 3 wt% Cr doped SnO_2 nanoparticles and (c and d) corresponding HRTEM images.

TEM measurements were performed to confirm the nanocrystalline nature of the samples, to examine the morphology, and also to check for impurities if any at the nanoscale. Typical TEM micrographs and high-resolution (HRTEM) images of undoped and 3 wt% Cr doped SnO_2 samples are shown in Fig. 2. The results show that they have spherical like morphology with average particle sizes of 21 and 16 nm respectively. The average crystallites size estimated from the XRD pattern is in good agreement with the TEM results. The HRTEM image for undoped and 3 wt% Cr doped SnO_2 nanoparticles are shown in Fig. 2c and d. Undoped SnO_2 nanocrystallites exhibit highly symmetrical and sharp lattice lines which confirm their single

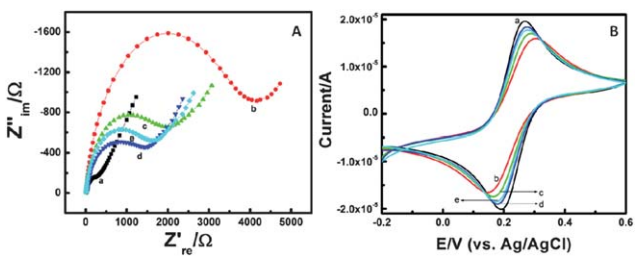

Fig. 3 (A) EIS behaviour of the modified GCE measured by impedance in the frequency region from 100 kHz to 1 Hz at a DC potential of 250 mV and AC potential of ± 5 mV in the presence of 1 mM $[Fe(CN)_6]^{3-/4-}$ in 0.1 M KCl. (B) CV behaviour of the modified GCE measured in presence of 1 mM $[Fe(CN)_6]^{3-/4-}$ in 0.1 M KCl at a scan rate of 50 mV s^{-1}. Curve a: bare GCE, curve b: pure SnO_2, curve c: 1 wt%, curve d: 3 wt% and curve e: 5 wt% Cr doped nano-SnO_2 modified electrodes. The optimized concentration (6 mg mL^{-1}) was used for electrode modification.

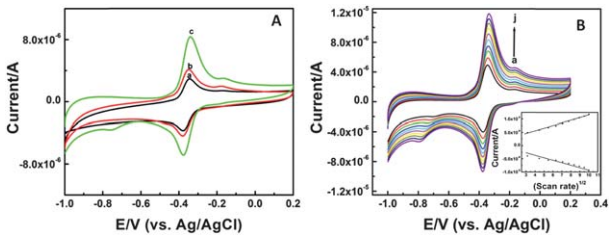

Fig. 4 (A) CVs obtained for RF (100 μM) at the (a) bare, (b) nano-SnO_2 and (c) nano-Cr–SnO_2 modified electrode recorded in PBS (pH 5.0) at a scan rate of 50 mV s^{-1} at a potential between −1.0 and 0.2 V and (B) CVs obtained for RF (100 μM) at the nano-Cr–SnO_2 modified electrode at different scan rates (10–100 mV s^{-1}) in PBS (pH 5.0). The optimized concentration (6 mg mL^{-1}) was used for electrode modification.

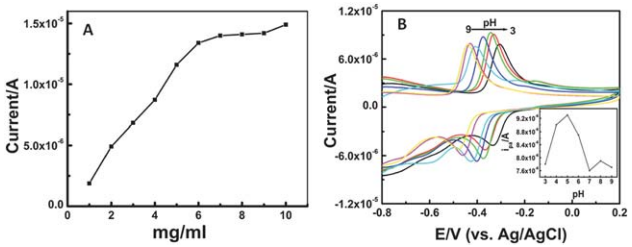

Fig. 5 (A) Effect of film thickness of nano-Cr–SnO_2 (1–10 mg mL^{-1}) on CV signals of RF (100 μM) in PBS (pH 5.0) with a potential window of −1.0 to 0.2 V at a scan rate of 50 mV s^{-1} and (B) CVs of the nano-Cr–SnO_2 modified electrode in PBS (pH 3.0–9.0) containing 100 μM of RF at a scan rate of 50 mV s^{-1}. Inset shows plot of oxidation peak current of RF *vs.* pH.

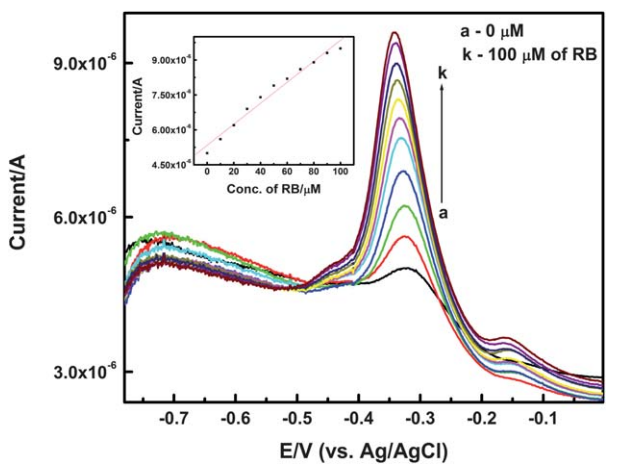

Fig. 6 LSVs obtained for RF in the concentrations ranging from 10 to 100 μM. RF was added in steps of 10 μM each at the nano-Cr–SnO_2 modified electrode in PBS (pH 5.0).

crystalline and defect free nature. However, Cr-doping seems to introduce twin-like defects in the crystallites (Fig. 2d). Further, HRTEM pictures did not indicate the presence of any secondary phase or trace elements present in the samples.

3.2 Magnetic measurements

Magnetization measurements on pure and Cr doped SnO_2 nanoparticles annealed at 600 °C were performed using a

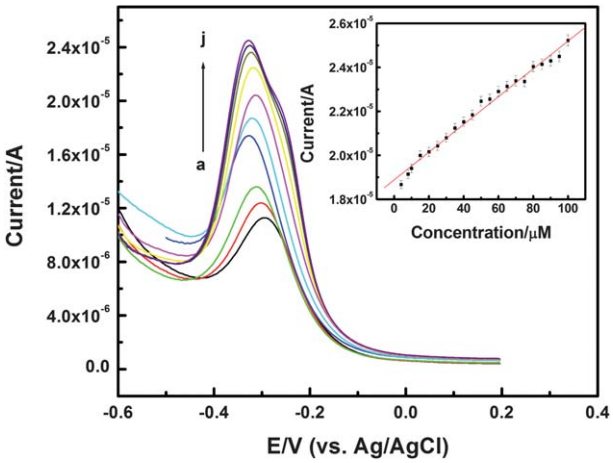

Fig. 7 DPVs of the nano-Cr–SnO_2 modified GC electrode in nitrogen saturated PBS (pH 5.0) with various concentrations of RF (a–j) 0, 0.2 × 10^{-6}, 0.5 × 10^{-6}, 4.0 × 10^{-6}, 8.0 × 10^{-6}, 1.0 × 10^{-5}, 3.0 × 10^{-5}, 5.0 × 10^{-5}, 8.0 × 10^{-5} and 1.0 × 10^{-4} M; scan rate 0.020 V s^{-1}; amplitude 0.05 V and step potential 0.07 V. Inset shows the resulting calibration plot.

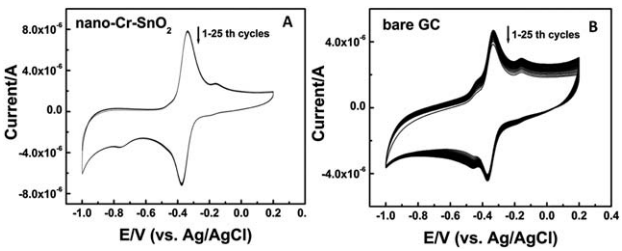

Fig. 8 (A) CVs stability of nano-Cr–SnO_2 modified GCE and (B) bare GC in PBS containing 100 μM of RF at a scan rate of50 mV s^{-1}.

vibrating sample magnetometer at room temperature. Magnetization *M versus* field *H* curves are presented in Fig. S1.† Undoped SnO_2 showed the expected diamagnetic behaviour with negative susceptibility. The diamagnetism arises due to the 4+ valance state of tin (Sn^{4+}) which favours the $4d^{10}$ electronic configuration in SnO_2 and hence, there are no unpaired d electrons in the structure for any kind of ferromagnetic ordering.[28] 1 wt% Cr doping did not change the diamagnetic nature of the SnO_2. But the 3 wt% Cr doped SnO_2 exhibits good ferromagnetic behaviour at room temperature. The saturation magnetization (M_s) and coercive field (H_C) of Cr (3 wt%) doped SnO_2 nanoparticles are estimated to be about 7.5 × 10^{-3} emu g^{-1} and 253 kOe respectively. At 5 wt% Cr, the M_s value is noticeably enhanced to 20.56 × 10^{-3} emu g^{-1}, almost three times higher than the value of the 3 wt% Cr doped SnO_2 sample. Though numerous work has been done on the transition metal doped SnO_2, the mechanism responsible for the origin of ferromagnetism at room temperature still remains controversial. So far, several assumptions such as the role of the secondary phase, the connection between defects and magnetism, oxygen vacancy, *etc* have been proposed to explain the origin of ferromagnetism in SnO_2.[29] Before ascribing the observed room temperature ferromagnetism (RTFM) to be

Table 1 Determination of RF in pharmaceutical and nutrition products

Sample	Labelled content (mg per tablet)	Observed content with DPV (mg per tablet)	RSD ($n = 3$) (%)
Riboflavin tablet	10	9.45 ± 0.08	1.21
B complex tablet	10	9.73 ± 0.05	0.87
Milk powder	—	6.72 ± 0.12	2.38

intrinsic, one should rule out the possibility that the impurity phase is responsible for the ferromagnetism. Powder XRD and HRTEM studies ruled out the possibility of impurity phases, particularly ferromagnetic CrO_2 phase. Therefore, based on the discussion above, we confirmed a uniform incorporation of Cr into SnO_2 without any secondary phase and suggested that the Cr^{3+} ions substitution for Sn^{4+} ions results in the creation of oxygen vacancies in order to ensure charge neutrality. The presence of a certain amount of such oxygen vacancies plays an important role in promoting the RTFM. For 5 wt% Cr, we do not observe any hysteresis behaviour at 300 K (inset of Fig. S1†) indicating loss of weak ferromagnetic behaviour with increasing Cr concentration.[30]

In the present work, we demonstrate that the ferromagnetic Cr–SnO_2 nanoparticles is useful for the sensitive and selective detection of RF with a high electrocatalytic activity toward RF sensing when compared to that of other nanoparticles.

3.3 EIS and CV studies on nano-Cr–SnO_2 modified GCE

It is well known that EIS is a powerful tool for studying the surface properties of modified electrodes. The charge transport process of the nano-Cr–SnO_2 modified GCE was studied by monitoring charge transfer resistance (R_{CT}) at the electrode–electrolyte interface. Fig. 3A shows the EIS curves of the bare and modified GCEs. The value of the charge transfer resistance (R_{CT}) for the bare GCE, undoped SnO_2, 1 wt%, 3 wt% and 5 wt% Cr doped nano-SnO_2 modified GCEs were estimated to be 281, 3685, 1808, 1256 and 1449 Ω cm^{-2}, respectively. The R_{CT} value of 3 wt% Cr doped nano-SnO_2 modified GCE is much lower than that of the undoped and the other Cr (1 and 5 wt%) doped nano-SnO_2 modified GCEs. Upon increasing the Cr content to 5 wt%, the R_{CT} value increased in agreement with the fact that Cr^{3+} substitution at the Sn^{4+} site minimizes electron density in the n-type semiconductor SnO_2. It should be remembered that the Cr doping induces the magnetic phase transition from diamagnetic (undoped and 1 wt% Cr doped SnO_2) to ferromagnetic nature (Cr 3 wt%). The observed enhancement in the charge transport characteristic of 3 wt% Cr doped SnO_2 is in agreement with the proposal that the doping induced oxygen vacancy plays an important role in the charge transport and magnetic behaviour of nano-SnO_2. These results collectively indicated that the 3 wt% Cr doping into SnO_2 is the saturation point and it is facilitating the charge transport between the modified electrode surface and redox couple. Hence we have used 3 wt% Cr doped SnO_2 nanoparticles for further investigation and it is represented as nano-Cr–SnO_2.

The CVs of the undoped and Cr doped nano-SnO_2 modified electrodes recorded in the presence of 1 mM $Fe(CN)_6]^{3-/4-}$ in 0.1 M KCl at a scan rate 50 mV s^{-1} are shown in Fig. 3B. At the bare GCE (curve a), a pair of well defined redox peak was observed with a peak separation of 70 mV ($\Delta E_p = (E_{pa} - E_{pc})$). But, for the undoped SnO_2 (curve b), 1 wt% (curve c), 3 wt% (curve d) and 5 wt% (curve e) Cr doped nano-SnO_2 modified electrodes, the peak to peak separation values (ΔE_p) were estimated to be 162, 123, 96 and 103 mV, respectively. The undoped and Cr (1 and 5 wt%) doped nano-SnO_2 modified GCEs showed larger ΔE_p values compared to that of the 3 wt% Cr doped nano-SnO_2 modified GCE. The larger peak separation was assumed to result from the lower electrical conductivity. These results are in good agreement with the charge transfer resistance values obtained from EIS measurements.

3.4 Electrocatalytic oxidation of RF

The CVs of (a) bare GCE, (b) nano-SnO_2 and (c) nano-Cr–SnO_2 modified GCEs recorded in nitrogen saturated PBS (pH 5.0) containing 100 μM of RF at a scan rate of 50 mV s^{-1} are shown in Fig. 4A. Compared to those obtained at the bare GCE (2.9×10^{-6} A) and nano-SnO_2 (4.1×10^{-6} A) modified GCEs, a remarkably larger peak current was obtained at the nano-Cr–SnO_2 modified GCE (8.3×10^{-6} A). This anodic peak current (i_{pa}) obtained for the nano-Cr–SnO_2 modified electrode is nearly 3 and 2 fold higher when compared to the bare GCE and nano-SnO_2 modified electrodes, respectively. It is also noted that the peak to peak separation (ΔE_p) of the bare GCE is higher (40 mV) than that of the undoped SnO_2 and nano-Cr–SnO_2 modified GCEs (30 mV). The nano-Cr–SnO_2 modified electrode did not show any redox peak in the absence of RF (data not shown). These data indicate that the nano-Cr–SnO_2 has a good electrocatalytic effect towards RF sensing compared to that of the bare GCE and undoped nano-SnO_2.

Fig. 4B shows the CVs of the nano-Cr–SnO_2 (3 wt% Cr) modified GCE recorded at different scan rates (10–100 mV s^{-1}) in nitrogen saturated PBS (pH 5.0) containing 100 μM of RF. Both the oxidation and reduction peak heights of the redox process were found to increase linearly with the square root of the scan rate from 10 to 100 mV s^{-1}. The regression equation was deduced to be I_{pa} (μA) = 1.01 (V^{-1} s^{-1}) + 1.36, $r = 0.996$; I_{pc} (μA) = −0.72 (V^{-1} s^{-1}) − 1.41, $r = 0.990$. This indicated that the electrode reaction of RF was under diffusion control. Further, it involves two electron and two proton reactions in the electrocatalysis reversible reduction of RF at the nano-Cr–SnO_2 modified GCE and is represented as follows.

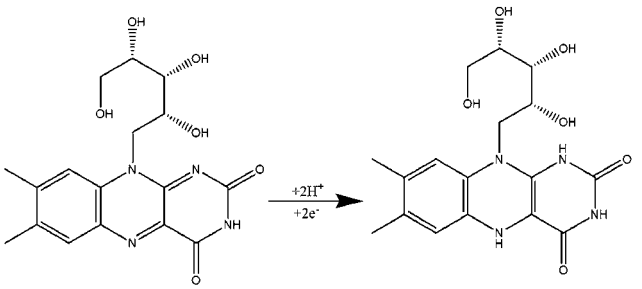

Further, optimization of film thickness and pH for the nano-Cr–SnO_2 modified electrode in PBS containing 100 μM of RF was carried out (Fig. 5.). The influence of film thickness of nano-Cr–SnO_2 (1–10 mg mL^{-1}) on RF (100 μM) sensing was investigated by CV at a scan rate of 50 mV s^{-1}, and the results are shown in Fig. 5A. From this figure, we can observe that the oxidation peak current (i_{pa}) signal of RF is the strongest when the thickness of the nano-Cr–SnO_2 film was 6 mg mL^{-1}.

The influence of pH on the electrochemical behaviour of RF (100 μM) at the nano-Cr–SnO_2 modified electrode was examined by recording CVs in PBS (pH 3.0–9.0) at a scan rate of 50 mV s^{-1}. The results are shown in Fig. 5B, where it can be seen that redox peaks of RF at the nano-Cr–SnO_2 modified surface shifted negatively with increasing pH. Further, the results show that the electrode potential of the redox peaks strongly depend on the pH of the electrolyte. All changes in CV peak potentials and currents with pH were reversible. When the pH of the PBS was 5.0, the oxidation peak current (i_{pa}) of RF responded strongly, yielding a maximum RF oxidation peak current of 9.30×10^{-6} A (inset of Fig. 5B). Therefore, a PBS with pH 5.0 was chosen for the rest of the electrochemical sensing of RF in this work.

Fig. 6 shows the linear sweep voltammograms (LSVs) obtained for RF in the concentration range of 10–100 μM at the nano-Cr–SnO_2 modified electrode. The oxidation current of RF increased with a slight negative potential shift in the oxidation peak potential upon each increment of 10 μM. The oxidation currents had a linear relationship with the concentration of RF with a correlation coefficient of 0.990 (inset of Fig. 6).

Furthermore, DPV was performed to examine the sensitivity of the nano-Cr–SnO_2 modified electrode towards the detection of RF. Fig. 7 depicts the DPV curves of the nano-Cr–SnO_2 modified electrode in PBS (pH 5.0) for different concentrations of RF. Here the DPVs were recorded by sweeping the potential between −1.0 and 0.2 V at an amplitude of 0.05 V, a step potential of 0.07 V and a scan rate of 20 mV s^{-1}. In Fig. 7, curves a–j show the well-defined and stable anodic oxidation peak current curves for RF. These results demonstrated that the nano-Cr–SnO_2 modified electrode might provide a good electrocatalytic activity towards RF sensing. The DPVs current linearly increased when the concentration of RF was increased from 0.2×10^{-6} to 1.0×10^{-4} M at the nano-Cr–SnO_2 modified electrode with a correlation coefficient of 0.9935. The detection limit was found to be 107 nM (inset of Fig. 7).

3.5 Selective determination of RF in the presence of interfering compounds using the nano-Cr–SnO_2 modified electrode

The anti-interference ability was tested by DPV of the nano-Cr–SnO_2 modified electrode towards the detection of RF in the presence of various common ions such as Fe^{3+}, Mg^{2+} and Ca^{2+} and some physiological interferents such as L-ascorbic acid and uric acid. No change in the DPV current response was observed for 10 μM RF in the presence of 1000 μM of $FeCl_3$, $MgSO_4$ and $CaCl_2$; and 100 μM of L-ascorbic acid and uric acid. Results summarized in ESI Table S2† show that the present modified electrode is highly selective towards the determination of RF even in the presence of 100-fold excess of these interferents.

3.6 The stability and reproducibility of the nano-Cr–SnO_2 modified electrode

In order to investigate the stability of the nano-Cr–SnO_2 modified electrode by CV in PBS (pH 5.0) containing 100 μM of RF; 25 continuous cycles were carried out at a scan rate of 50 mV s^{-1}. The results show only a 1.71% loss from the initial value, whereas the bare GCE exhibits almost 18.01% loss after 25 cycles (Fig. 8). These results indicate that the nano-Cr–SnO_2 modified electrode has a good stability, reproducibility and does not undergo surface fouling. To ascertain the reproducibility of the results, four different GCEs were modified with the nano-Cr–SnO_2 and their response towards the oxidation of 1.0 μM RF was tested. The peak current obtained in the measurements of three independent electrodes showed a relative standard deviation of 6.55%, confirming that the results are reproducible. The above results show that the fabricated RF sensor is very stable and reproducible.

The main advantages of the newly fabricated RF sensor is that the metal oxide preparation (microwave irradiation method) and electrode modification (drop cast method) procedure adopted in the present study is very simple when compared to the literature methods.[25,31,32] Moreover, the fabricated nano-Cr–SnO_2 modified electrode is more sensitive and selective towards the determination of RF in the presence of 10-fold L-ascorbic acid, uric acid and 100 fold Fe^{3+}, Mg^{2+} and Ca^{2+}. The performance of the fabricated RF sensor is very much comparable to the literature values (ESI Table S3†). The comparative data suggests superiority of the present sensor over some reported RF sensors, the possible reason being that the ferromagnetic behaviour of the nano-Cr–SnO_2 coupled with high surface area and good electrocatalytic activity. The doping induced twin-like defects in the 3 wt% Cr doped SnO_2 nanoparticles can also partially be responsible for the enhanced sensitivity of the RF sensors.

3.7 Determination of RF in real samples

The practical application of the nano-Cr–SnO_2 modified electrode was tested by measuring the concentration of RF in pharmaceutical and milk powder samples. Pursuing the proposed method, the concentration of RF in two different pharmaceutical preparations was ascertained and the results

are summarized in Table 1. The data shows that the RF content in the examined tablets and milk powder fall within the tagged amount suggesting the good applicability of the proposed voltammetric method.

4 Conclusions

We have successfully synthesized Cr (0, 1, 3, and 5 wt%) doped SnO_2 nanoparticles by the microwave irradiation method. The rutile structure of SnO_2 was confirmed by X-ray diffraction and TEM studies, and no presence of Cr metals or other magnetic phases could be detected. The 3 wt% Cr doped SnO_2 nanoparticles exhibit room temperature ferromagnetism which was attributed to the possible enhancement of oxygen vacancies in the parent compound SnO_2. We have fabricated a highly sensitive RF sensor based on a Cr doped SnO_2 nanoparticles modified electrode for the first time using DPV. Compared with undoped SnO_2, the Cr (3 wt%) doped SnO_2 modified electrode exhibits improved catalytic activity toward the detection of RF. Excellent performance in sensitivity, stability, selectivity, reproducibility and freedom from interference was achieved when the sensor was exposed to RF solution. All these advantageous features can make the proposed sensor applicable in medical, food or other areas.

Acknowledgements

CS and NL acknowledge the University Grants Commission (UGC. F. no. 40-2/2011) for the financial assistance. The authors thank Dr P. Manisankar and Dr V. Yegnaraman for their help in DPV measurement and discussion.

Notes and references

1 J. Wang, *Analyst*, 2005, **130**, 421.
2 A. Bouaine, N. Brihi, G. Schmerber, C. Ulhaq-Bouillet, S. Colis and A. Dinia, *J. Phys. Chem. C*, 2007, **111**, 2924.
3 H.-J. Ahn, H.-C. Choi, K.-W. Park, S.-B. Kim and Y.-E. Sung, *J. Phys. Chem. B*, 2004, **108**, 9815.
4 H.-S. Kim, L. Bi, G. F. Dionne, C. A. Ross and H.-J. Paik, *Phys. Rev. B: Condens. Matter Mater. Phys.*, 2008, **77**, 214.
5 R. Kalai Selvan, I. Perelshtein, N. Perkas and A. Gedanken, *J. Phys. Chem. C*, 2008, **112**, 1825.
6 S. K. Misra, S. I. Andronenko, S. Rao, S. V. Bhat, C. Van Komen and A. Punnoose, *J. Appl. Phys.*, 2009, **105**, 07C514.
7 K. Nomura, J. Okabayashi, K. Okamura and Y. Yamada, *J. Appl. Phys.*, 2011, **110**, 083901.
8 A. K. Mishra, T. P. Sinha, S. Bandyopadhyay and D. Das, *Mater. Chem. Phys.*, 2011, **125**, 252.
9 H. Kimura, T. Fukumura, H. Koinuma and M. Kawasaki, *Phys. E.*, 2001, **10**, 265.
10 G. Korotcenkov and S. D. Han, *Mater. Chem. Phys.*, 2009, **113**, 756.
11 S. A. Ahmed, *Solid State Commun.*, 2010, **150**, 2190.
12 F. H. Aragón, J. A. H. Coaquira, P. Hidalgo, S. L. M. Brito, D. Gouvea and R. H. R. Castro, *J. Non-Cryst. Solids*, 2010, **356**, 2960.
13 L. Fang, X. Zu, C. Liu, Z. Li, G. Peleckis, S. Zhu, H. Liu and L. Wang, *J. Alloys Compd.*, 2010, **491**, 679.
14 H. J. Powers, *Am. J. Clin. Nutr.*, 2003, **77**, 1352.
15 A. A. Ensafi, E. Heydari-Bafrooei and M. Amini, *Biosens. Bioelectron.*, 2012, **31**, 376.
16 C. J. Bates, *Riboflavin, MRC Human Nutrition Research*, Cambridge, UK, Elsevier Ltd, 2005, p. 100.
17 B. J. Petteys and E. L. Frank, *Clin. Chim. Acta*, 2011, **412**, 38.
18 H. Qi, Z. Cao and L. Hou, *Spectrochim. Acta, Part A*, 2011, **78**, 211.
19 T. Perez-Ruiz, C. Martinez-Lazazo, V. Tomas and O. Val, *Analyst*, 1994, **119**, 1199.
20 S. M. Mandal, M. Mandal, A. K. Ghosh and S. Dey, *Anal. Chim. Acta*, 2009, **640**, 110.
21 E. J. Llorent-Martınez, J. F. Garcia-Reyes, P. Ortega-Barrales and A. Molina-Diaz, *Anal. Chim. Acta*, 2006, **555**, 128.
22 B. Janik and P. J. Elving, *Chem. Rev.*, 1968, **68**, 295.
23 R. M. Kotkar, P. B. Desai and A. K. Srivastava, *Sens. Actuators, B*, 2007, **124**, 90.
24 H. Y. Gu, A. M. Yu and H. Y. Chen, *Anal. Lett.*, 2001, **34**, 2361.
25 A. Safavi, N. Maleki, H. Ershadifar and F. Tajabadi, *Anal. Chim. Acta*, 2010, **674**, 176.
26 L. Bandzuchova, R. Selesovska, T. Navratil, J. Chylkov and L. Novotny, *Electrochim. Acta*, 2012, **75**, 316.
27 N. Lavanya, S. Radhakrisnan and C. Sekar, *Biosens. Bioelectron.*, 2012, **36**, 41.
28 Z. M. Tian, S. L. Yuan, J. H. He, P. Li, S. Q. Zhang, C. H. Wang, Y. Q. Wang, S. Y. Yin and L. Liu, *J. Alloys Compd.*, 2008, **466**, 26.
29 C. B. Fitzgerald, M. Venkatesan, L. S. Dorneles, R. Gunning, P. Stamenov, J. M. D. Coey, P. A. Stampe, R. J. Kennedy, E. C. Moreira and U. S. Sias, *Phys. Rev. B: Condens. Matter Mater. Phys.*, 2006, **74**.
30 L. Zhang, S. Ge, Y. Zuo, J. Wang and J. Qi, *Scr. Mater.*, 2010, **63**, 953.
31 S. Y. Ly, H. S. Yoo, J. Y. Ahn and K. H. Nam, *Food Chem.*, 2011, **127**, 270.
32 J. Li, Y. Zhang, T. Yang, H. Zhang, Y. Yang and P. Xiao, *Mater. Sci. Eng., C*, 2009, **29**, 2360.